Naval Research Laboratory

Washington, DC 20375-5000 NRL Memorandum Report 5909 December 31, 1986

AD-A177 218

Electron Energy Deposition in Atomic Oxygen

S. SLINKER AND A. W. ALI

Plasma Physics Division
Naval Research Laboratory
Washington, DC 20375-5000

87 2 20 130

AD-A177 218

SECURITY CLASSIFICATION OF THIS PAGE

REPORT DOCUMENTATION PAGE

1a. REPORT SECURITY CLASSIFICATION: UNCLASSIFIED

1b. RESTRICTIVE MARKINGS:

2a. SECURITY CLASSIFICATION AUTHORITY:

2b. DECLASSIFICATION/DOWNGRADING SCHEDULE:

3. DISTRIBUTION/AVAILABILITY OF REPORT: Approved for public release; distribution unlimited.

4. PERFORMING ORGANIZATION REPORT NUMBER(S): NRL Memorandum Report 5909

5. MONITORING ORGANIZATION REPORT NUMBER(S):

6a. NAME OF PERFORMING ORGANIZATION: Naval Research Laboratory

6b. OFFICE SYMBOL (If applicable): Code 4700.1

6c. ADDRESS (City, State, and ZIP Code): Washington, DC 20375-5000

7a. NAME OF MONITORING ORGANIZATION: Naval Surface Weapons Center

7b. ADDRESS (City, State, and ZIP Code): Silver Spring, MD 20903-5000

8a. NAME OF FUNDING/SPONSORING ORGANIZATION: DARPA

8b. OFFICE SYMBOL (If applicable):

8c. ADDRESS (City, State, and ZIP Code): Arlington, VA 22209

9. PROCUREMENT INSTRUMENT IDENTIFICATION NUMBER:

10. SOURCE OF FUNDING NUMBERS

PROGRAM ELEMENT NO.	PROJECT NO.	TASK NO.	WORK UNIT ACCESSION NO.
6270E	60921-86-WR-W0231	A63 ARPA Order 4395	DN680-415

11. TITLE (Include Security Classification): Electron Energy Deposition in Atomic Oxygen

12. PERSONAL AUTHOR(S): Slinker, S. and Ali, A. W.

13a. TYPE OF REPORT: Interim

13b. TIME COVERED: FROM ______ TO ______

14. DATE OF REPORT (Year, Month, Day): 1986 December 31

15. PAGE COUNT: 37

16. SUPPLEMENTARY NOTATION:

17. COSATI CODES

FIELD	GROUP	SUB-GROUP

18. SUBJECT TERMS (Continue on reverse if necessary and identify by block number): Electron energy deposition; Oxygen atom; Energy per electron-ion pair; Secondary electron distribution

19. ABSTRACT (Continue on reverse if necessary and identify by block number)

approx.

The interaction of high energy electrons (E < 1 MeV) with atomic oxygen is described. A code for discrete energy deposition scheme was developed.

The discrete energy method provides the electron loss function in oxygen the secondary electron distribution, the mean energy per electron-ion pair generation, and the efficiencies of all relevant inelastic processes.

Our calculations show that high energy electrons (500-100,000 eV) expend 28 eV to generate an electron-ion pair.

20. DISTRIBUTION/AVAILABILITY OF ABSTRACT: ☒ UNCLASSIFIED/UNLIMITED ☐ SAME AS RPT. ☐ DTIC USERS

21. ABSTRACT SECURITY CLASSIFICATION: UNCLASSIFIED

22a. NAME OF RESPONSIBLE INDIVIDUAL: A. W. Ali

22b. TELEPHONE (Include Area Code): (202) 767-3762

22c. OFFICE SYMBOL: Code 4700.1

DD FORM 1473, 84 MAR — 83 APR edition may be used until exhausted. All other editions are obsolete

SECURITY CLASSIFICATION OF THIS PAGE

*U.S. Government Printing Office: 1985-507-047

TABLE OF CONTENTS

1.	Introduction	1
2.	The Secondary Electron Distribution	3
2.1	The Source Term S(E,t)	4
2.2	Electron Impact Excitation Cross Section	5
2.3	Energy Loss to Plasma Electrons	7
3.0	Results	7
3.1	The Loss Function for Electrons with $E > 10^6$ eV	7
3.2	The Loss Function for Electrons with $E < 10^6$ eV	8
4.0	Comparison and Discussion	9
5.	References	11

ELECTRON ENERGY DEPOSITION IN ATOMIC OXYGEN

1. Introduction:

High energy electrons interacting with gaseous elements produce secondary electrons which in turn generate additional ionization. A simple description of the cumulative ionization in the gas, can be made if one knows w_i the energy expended by the electron in generating an ion pair. For example, in air, the energy expended to generate an ion pair is ~ 34 eV. In order to obtain w_i theoretically one must perform a detailed electron energy deposition in the gas. Such a deposition, in principle, provides an abundant amount of information. It will provide the secondary electron distribution, its flux, primary and secondary electron excitation rates for the internal modes of the atom or molecule (electronic, vibrational, etc.), w_i, and hence the total ionization rate. Accordingly electron energy deposition models in gaseous elements are essential and very useful in various applications; electron beam propagation in the atmosphere, electron beam generated lasers, electron beam generated discharges and their diagnostics, precipitation of energetic electrons in the upper atmosphere and auroral emissions.

There are many approaches to the electron energy deposition which may be classified[1] as follows:

1) Transport versus local description,

2) Continuous slowing down approximation versus discrete energy deposition, and

3) Transport or local energy loss versus Monte Carlo approach.

An extensive literature on this subject exists, however, we allude briefly to

Manuscript approved October 21, 1986.

some of them. For example, Green[2,3,4] and his colleagues have used the continuous slowing down approximation to calculate electron energy deposition in atmospheric and other gaseous elements. This method has been improved[1,5-10] by including discrete energy deposition for electrons with energy below 500 eV. Monte Carlo[11] and Fokker-Planck[12] methods have been utilized for energy deposition and the determination of the spatial distribution of the primary electrons. Boltzmann[13-15] equation solutions have also been utilized to obtain the equilibrium distribution of the secondary electrons.

In this paper we present a model for the energy deposition in the atomic oxygen, obtain the secondary electron distribution, the efficiency of excitation to various electronic states and ionization continua and the mean energy expended for ion pair production. This effort requires, at the outset, a set of electron impact excitation and ionization cross sections for atomic oxygen. These cross sections are essential for electron energy deposition schemes and are presented in detail.

Electron deposition claculations in atomic oxygen have been performed by Dalgarno and Lejeune[9] for the photoelectrons in the ionosphere. These photoelectrons are produced through the absorption of the solar radiation by oxygen and generally are low energy electrons ~ 100 eV. Accordingly a discrete energy deposition scheme is utilized.[9] In their treatment electron energy dissipation to the plasma (thermal) electrons is also included. Ganas and Green[16] have calculated loss function, L(E), in oxygen for electrons with energy $E < 5$ KeV. However, energy loss to plasma electrons is not considered and the range of the primary electrons (≤ 10 KeV) is higher than those considered by Dalagaro and Lejeune.[9] Singhal and Green[17] have considered the spatial aspects of electron energy degradation using Monte Carlo approaches for electron energies below 10 KeV. Our interest, however, is in the

interaction of high energy and high current electron beams with oxygen ($E > 10$ KeV). Accordingly, we utilize a new code for energy deposition in gaseous species. This code is similar in numerics to an earlier code developed at NRL[1] and has the capability to treat the super elastic collisions and its effects on the plasma electron velocity distribution, in a manner similar to that of Ref. 18.

2. The Secondary Electron Distribution:

The secondary electron distribution can be calculated[1] from Eq. 1

$$\frac{\partial N_e(E,t)}{dt} = S(E,t) - N\sum_k \sigma_k(E)\, V(E)\, N_e(E,t)$$
$$+ N \sum_k \int \sigma_k(E',E)\, V(E')\, N_e(E',t)dE'$$
$$+ N_p(t) \frac{\partial}{\partial E} [\, L_p(E)V(E)\, N_e(E,t)\,] \qquad (1)$$

where $N_e(E,t)$ is the secondary electron density per unit volume per unit energy ($cm^{-3}eV^{-1}$) and $S(E,t)$ the production rate ($cm^{-3}sec^{-1}eV^{-1}$) due to primary electrons. The second term in the right hand side of Eq. 1 indicates the loss of the secondary electrons with energy E due to inelastic collisions resulting in excitations where the cross section for the kth excitation is denoted by $\sigma_k(E)$, $V(E)$ the electron velocity and N the density of the atomic oxygen. The third term in Eq. (1) represents the production of a secondary electron of energy E by a higher energy electron of energy E'. The differential ionization cross section for this process is $\sigma_k(E',E)$ with the index k denoting the kth ionization continuum of oxygen. The energy loss to plasma electrons, N_p, is given by the last term on the right hand side of Eq. 1., where $L_p(E)$ is the loss function of a secondary electron with energy E to the plasma electrons. We select the bulk of the plasma electrons to be those with energy between 0.04-1.96 eV, where 1.96 eV denotes the threshold of the

excitation of the lowest oxygen electronic state (^1D). The various terms appearing in Eq. 1 are discussed in detail below.

2.1. The Source Term S(E,t)

The emphasis in this paper is on high energy electron beam deposition in oxygen. Therefore, the source term for the generation of the secondary electrons is

$$S(E,t) = j_b(E_b)\sigma_b(E_b,E)\ N \tag{2}$$

where $j_b(E_b)$ is the number density of the beam electrons whose energy is E_b and $\sigma_b(E_b,E)$ is the differential ionization cross section. The differential ionization cross section has been measured for many molecules and atoms by Opal et al,[19] for primary electrons with energy of 2000 eV and lower. However, no measurement for atomic oxygen is available. On the other hand, Opal et al[19] have observed that most of their data for the differential ionization cross section can be expressed as

$$\sigma(E_p,E_s) = C(E_p)\ [1 + (E_s/\varepsilon)^2\ ]^{-1} \tag{3}$$

where E_p is the energy of the primary electron, $C(E_p)$ a constant obtained by Eq. (4).

$$\sigma_i(E_p) = \int_0^{\frac{E_p-I}{2}} \sigma(E_p,E_s)dE_s \tag{4}$$

and ε is an average energy characteristic of each species. $\sigma_i(E_p)$ denotes the total ionization cross section for electrons with energy E_p and I the ionization energy of the atom. Therefore, one may use Eq. (3) and (4) with an

assumed value for ε and the most recent measured[20] values of the total ionization cross section and obtain $C(E_p)$. The total cross section measurements in general are for electron energies up to 1000 eV. Strickland, et al[13] have used the following expression for the differential ionization cross section for oxygen.

$$\sigma(E_p,E_s) = \frac{2}{E_p-I}\,\sigma_I(E_p) \text{ for } E_p < I+10 \tag{5a}$$

$$\sigma(E_p,E_s) = C(E_p)\left\{\frac{1}{\varepsilon^2+25} + \frac{1}{\varepsilon^2+(E_p-I-5)^2}\right.$$

$$\left. - \frac{1}{\varepsilon^2+5(E_p-I-5)}\right\}, \text{ for } \begin{array}{l} E_b \geq I+10 \\ E_s \leq 5 \end{array} \tag{5b}$$

$$\sigma(E_p,E_s) = C(E_p)\cdot\left\{\frac{1}{E_s^2+\varepsilon^2} + \frac{1}{\varepsilon^2+(E_p-I-E_s)^2}\right. \tag{5c}$$

$$\left. - \frac{1}{\varepsilon^2+E_s(E_p-I-E_s)}\right\}, \text{ for } \begin{array}{l} E_p \geq I+10 \\ E_s > 5 \end{array}$$

However, for relativistic electrons one must use Moellers' formula.[21]

To obtain the fractional ionization leading to various ionization continuua i.e., $O^+(^4S)$, $O^+(^2D)$ and $O^+(^2P)$ we use the fractions obtained by Dalgarro and Lejeune[9]. Using these fractions we give the total and the fractional ionization cross sections as a function of the electron energy, (see Table 1).

2.2 Electron Impact Excitation Cross Section

In discussing the electron impact excitations of oxygen electronic states, one may divide the excitations into several categories. First, the low lying metastable states of oxygen $O(^1D)$ and $O(^1S)$ which belong to the

ground state configuration of the atom. These cross sections have been calculated by numerous workers (for details see Ref. 22) and those by Thomas and Nisbet,[23] which are preferred,[22] are shown in Fig. 1 and are given in Table II. The second group of electronic states are those with dipole allowed transitions to the ground state. For these states, the following expression given by Drawin,[24] can be used.

$$\sigma_{ij} = 3.5\times10^{-16}\, f_{ij} \left(\frac{13.6}{E_{ij}}\right)^2 \left(\frac{E_{ij}}{E}\right)^2 \left(\frac{E}{E_{ij}} - 1\right) \log\left(1.25\, \frac{E}{E_{ij}}\right) \quad (6)$$

Here, f_{ij} is the oscillator strength for the transition from state i to j whose excitation energy is E_{ij}. Using Eq. 6 the electron impact excitation for the transition $^3p \rightarrow {}^3s$ (the resonance line) is shown in Figure 2. The experimental data for the absolute cross section[25,26] is also shown in Fig. 2 along with other theoretical[27-29] calculations. It is obvious that the experimental data is higher than the theortical calculations because the experimental data includes cascade from higher states. However, we normalize our calculations to 0.5 of the experimental value making our result in good accord with Ref. 27. The appropriate parameters for the optically allowed transitions are given in Table III.

For forbidden transitions e.g. ^3p-$^5s^0$ we utilize the experimental data[26] (see Table IV). For higher states we use the parametric fits developed by Jackman et al[30] where the cross section is expressed as

$$\sigma_{ij} = \frac{6.5\times10^{-14} C f_{ij}}{E_{ij}^2} \left(1 - \frac{E_{ij}}{E}\right)^{\nu} \left(\frac{E_{ij}}{E}\right)^{\Omega} \quad (7)$$

and the appropriate parameters are given in Table V.

As for higher Rydberg states, we obtain the asympotic values of the oscillator strength usin[illegible] the quantum defect method. For these and other states included in the e[illegible] deposition, see Table V and Fig. 3.

2.3. Energy Loss to Plasma Electrons:

Perkins[31] has derived the rate of energy loss to plasma electrons by a test electron. These results have been utilized by Schunk and Hays[32] to obtain the following expressions for the energy loss

$$\frac{dE}{dt} = \frac{\omega_p^2 e^2}{V^2} \log \frac{mV^3}{\gamma e^2 \omega_p} \qquad \text{for} \quad kT << E << \frac{me^4}{2\hbar^2} \tag{8}$$

$$= \frac{\omega_p^2 e^2}{V^2} \log \frac{mV^2}{h\omega_p} \qquad \text{for} \quad E > \frac{me^4}{2\hbar^2} \tag{9}$$

where ω_p is the plasma frequency. These can be expressed, in terms of the loss function (see Eq. 1), as

$$L_p(E) = \frac{1.3\text{x}10^{-13}}{E} \log \frac{8.2\text{x}10^9 E^{1.5}}{\sqrt{N_p}}, \qquad E < 20 \text{ eV} \tag{10}$$

$$L_p(E) = \frac{1.3\text{x}10^{-13}}{E} \log \frac{5.4\text{x}10^{10}}{\sqrt{N_p}} E, \qquad E > 20 \text{ eV} \tag{11}$$

3.0. Results:

3.1. The Loss Function For Electrons with $E > 10^6$ eV.

For electrons with energy above $E = 10^6$ we utilize the Bethe-Bloch[33] equation to calculate the stopping power. The relativistic form of the loss function[33] is

$$L(E) = \frac{2\pi r_o^2 mc^2}{\beta^2} Z \left[\log \frac{T^2}{I^2} \frac{(\gamma+1)}{2} + 1-\beta^2 - \frac{2\gamma-1}{\gamma^2} \log 2 + \frac{1}{8} \left(\frac{\gamma-1}{\gamma}\right)^2 \right] \tag{12}$$

Where r_o is the classical electron radius, Z the atomic number, T the kinetic energy of the electron and E the total energy and I the mean excitation energy which is equal to 89 eV for oxygen. We have used Eq. (12) to calculate the loss function in oxygen for T = 100 MeV down to $T = 10^4$ eV and show the result in Figure 3. It should be noted that our results are in good agreement with the calculations of Pages et al.[34] However, using Eq. 12 to obtain the loss function one obtains only the information on the energy loss per unit path. One does not obtain any other information e.g. the secondary electron distribution, its flux, the efficiency of excitation of individual excitation channels, and the energy per ion pair. Accordingly, our discrete deposition scheme does provide this relevant information.

3.2. The Loss Function for Electrons With $E < 10^6$ eV

The discrete energy deposition scheme described in detail in this report is utilized for primary electrons with $E < 10^6$ eV and the results are discussed in this Section. The loss function can be written as in Eq. (13).

$$L(E) = \sum_j W_j \sigma_j(E) + \sum_j I_j \sigma_I(E) + \sum_j \int_0^{E_{sjmax}} E_s \sigma_{Ij}(E,E_s) dE_s \qquad (13)$$

where the first term is a sum over excited states with excitation energy W_j and cross section $\sigma_j(E)$; the second term is a sum over ionization states with ionization energy I_j and cross section $\sigma_{Ij}(E,E_s)$ and the third term sums the amount of energy going into the secondaries with $E_{sjmax} = (E - I_j)/2$ the maximum secondary energy and $\sigma_{Ij}(E,E_s)$ the differential ionization cross section for the jth ionization state. Using Eq. (13) we obtain L(E) and show the results for electron enegies of 500 to 10^6 eV. These results are shown in Table VI. The percentages of the loss function going into these three channels is described in Eq. (13) are also given in Table VI. Figure 4 shows a plot of L(E) and its three terms.

The third row of Table VI gives W_i the energy expended to create an ion pair. For a given beam and oxygen background the number of ion pairs created per cubic cm per second is $\frac{1}{W_i} \frac{dE}{dX} F$ where F is the beam flux in beam particles per cm^2 per sec. W_i is fairly constant throughout this energy range but increases dramatically for lower beam energies[9] because the ratio of the excitation cross section to the ionization cross section gets larger. The fourth and fifth lines of Table VI give the percentage of ion pairs created directly from ionization by a beam electron - called first generation secondaries - and those created in the ensuing cascade.

Figure 5 shows the steady state secondary electron distribution function N_e while Figure 6 shows the flux $\phi = Ne\ V$. In all cases the beam flux was $F = 1.99 \times 10^{18}$ electrons per cm^2 per sec and the background was 2.46×10^{19} atoms of oxygen per cm^3.

Finally Table VII gives the production efficiencies for all the states in the model. The production efficiency of a state is defined to be the number of excitations of that state per ion pair created. Therefore the creation rate for a state is given by $P \frac{1}{W_i} \frac{dE}{dX} F$ where P is the appropriate production efficiency.

4.0. Comparison and Discussion:

The loss function, L(E), calculated by the discrete method, shown in Fig. 4, is replotted in Fig. 7, for comparison with the results predicted by Bethe's non relativistic expression and the calculations of Ganas and Green[16]. The discrete calculation is lower than what is predicted by Bethe's equation. The disagreement is ~ 12% at $E = 10^4$ and 25% at the $E = 10^3$ eV. However, the results of Ref. 16 are higher than those predicted by Bethe's equation and our own calculation.

The energy per ion pair predicted by our code is ~ 28 eV over a wide electron energy range (500-100,000 eV). There is no data, as far as we know,

in these energy ranges. However, Dalgarno and Lejeune[9] use the discrete method for the total absorption of the photoelectrons ($E \ll 100$ eV) in the ionosphere. They predict a value of 29 eV per electron ion pair. To compare our results with those of Lalgarno and Lejeune[9] we ran our code for incident electrons of 100 and 50 eV for the case of a completely stopped electron, as done by Dalgarno and Lejeune.[9] Our results for the energy per ion pair are 33.6 eV and 40.4 eV, respectively compared to 29 and 34, read from Fig. 13 of Ref. 9, for the case of a very low ionization fraction present in the gas. These results are fairly comparable.

In comparing our results with those of Ganas and Green[16] we note that they utilize the concept of generalized oscillator strength in obtaining excitation and ionization cross sections. One reason for their L(E) being larger than ours can be traced to their higher expression for the ionization cross section compared to the experimental data, which we use. For example at $E = 10^2$ eV they predict an ionization cross section of 3×10^{-16} cm^2 compared to the experimental data[20] of 1.3×10^{-16} cm^2. Their ionization cross sections however, fits the experimental data much better at E = 5000 eV. Here, their results for L(E) is higher than ours by 15% while their L(E) at E = 100 eV is nearly twice of ours and also much higher than that predicted by Bethe's equation.

Dalgarno and Lejeune do not report the calculations of L(E), however, they do calculate certain excitation efficiencies of excited states, specifically those of $O(^1D)$. In comparing our calculations with those of Ref. 9 we find an excitation efficiency for $O(^1D)$ at E = 100 eV to be twice as large as theirs. This certainly is due to the fact that they use the calculated cross sections of Henry, et al[35], while we utilize the more recent calculations of Thomas and Nisbet[23] which we believe to be more accurate. We can not compare excitation efficiencies with Ganas and Green, because in the

first place they do not consider the forbidden states of oxygen ^1D, and ^1S, etc. Furthermore, in their evaluation of the contribution of energy deposited to excitation and ionization they indicate that most of the energy goes into ionization. Our result does not show such a phenomena. Indeed, in our calculations we see that considerable energy is stored in the ^1D state. This discrepancy may be due to the fact that Ganas and Green have ignored those, and other forbidden states of oxygen.

REFERENCES

1. D.J. Strickland and A.W. Ali, "A Code for the Secondary Electron Distribution in Air and Some Application," NRL Memo Report 4956 (1982).

2. A.E.S. Green and C.A. Barth, J. Geophys. Res. **70**, 1083 (1965).

3. R.S. Stolarski and A.E.S. Green, J. Geophys. Res. **72**, 3967 (1967).

4. H.S. Porter, C.H. Jackman and A.E.S. Green, J. Chem. Phys. **65**, 154 (1976) and references therein.

5. P.M. Banks, C.R. Chappell, A.F. Nagy, J. Geophys. Res. **79**, 1459 (1974).

6. D. Strickland and P.C. Kepple, NRL Memo Report 2779 (1974). AD779262

7. L.R. Peterson, Phys. Rev. **187**, 105 (1969).

8. T.E. Cravens, G.A. Victor, and A. Dalgarno, Planet Space Sci. **23**, 1059 (1975).

9. A. Dalgarno and G. Lejeune, Planet Space Sci. **19**, 1653 (1971).

10. J.L. Fox, A. Dalgarno, and G.A. Victor, Planet Space Sci. **25**, 71 (1977). M.J. Berger and S.M. Seltzer, J. Atm. Terr. Phys. **32**, 1015 (1970).

12. M. Walt, W.M. McDonald, and W.E. Francis, Physics of the Magnetosphere, Carovillano, et al., Eds., Springer, New York (1968), p. 534.

13. D.J. Stickland, D.L. Book, T.P. Coffey, and J.A. Fedder, J. Geophys. Res. **81**, 2755 (1976).

14. D.R. Shure and J.T. Verdeyen, J. Appl. Phys. **47**, 4484 (1976).

15. Yu.A. Medvedev and V.D. Khokhlov, Soviet Phys. Tech. Phys. **24**, 181 (1979) ibid 185.

16. P.S. Ganas and A.E.S. Green, J. Quant. Spectros. Rad. Transfer **25**, 265 (1981).

17. R.P. Singhal and A.E.S. Green, J. Geophys. Res. **86**, 4776 (1981).

18. S.D. Rockwood, J.E. Brau, W.A. Proctor, and G.H. Canavan, IEEE, J. Quant. Elect. QE9, 120 (1973).

19. C.B. Opal, W.K. Peterson, and E.C. Beaty, J. Chem. Phys. **55**, 4100 (1971) and C.B. Opal, E.C. Beaty, and W.K. Peterson, Atomic Data **4**, 209 (1972).

20. E. Brook, M.F.A. Harrison, and A.C.H. Smith, J. Phys. B. **11**, 3115 (1978).

21. C. Moller, Ann. Phys. **14**, 531 (1932).

22. A.W. Ali, "Excitation and Ionization Cross Sections for Electron Beam and Microwave Energy Deposition in Air," NRL Memo Report 4598 (1981). ADA103106

23. L.D. Thomas and R.K. Nisbet, Phys. Rev. **A11**, 170 (1975).

24. H.W. Drawin, Report European CEA, Fusion Controlee, Center d' Studes Nuceaires, 383 Fontenay-Aux-Roses, France (1966) Revised (1967).

25. E.J. Stone and E.C. Zipf, Phys. Rev. **A4**, 610 (1971).

26. E.J. Stone and E.C. Zipf, J. Chem. Phys. **60**, 4237 (1974).

27. A.D. Stauffer and M.R.C. McDowell, Proc. Phys. Soc. **89**, 289 (1966).

28. S.P. Roundtree and R.J.W. Henry, Phys. Rev. **A6**, 2106 (1972).

29. T. Sawada and P.S. Ganas, Phys. Rev. **A7**, 617 (1973).

30. C.H. Jackman, R.H. Garvey, and A.E.S. Green, J. Geophys. Res. **82**, 5081 (1977).

31. F. Perkins, Physics of Fluids **8**, 1361 (1965).

32. R.W. Schunk and P.B. Hays, Planet Space Sci. **19**, 113 (1971).

33. H. Bethe, Handbuch der Physik (Springer, Berlin) **24**, 273 (1953).

34. L. Pages, E. Bertel, H. Joffre, and L. Sklavenitis, Atomic Data **4**, 1 (1972).

35. R.J.W. Henry, P.G. Burke, and A.-L. Sinfailam, Phys. Rev. **178**, 218 (1969).

Table I — Ionization Cross Section of O

E	σ	a(13.6)	b(16.93)	c(18.62)
13.6	0 -	-	-	
17	2.1(-17)	2.1(-17)	-	-
20.4	3.37(-17)	2.2(-17)	0.95(-17)	0.18(-17)
23.8	4.64(-17)	3.04(-17)	1.3(-17)	0.26(-17)
27.2	5.89(-17)	3.03(-17)	2.0(-17)	0.85(-17)
30.6	7.05(-17)	3.27(-17)	2.54(-17)	1.23(-17)
34	8.1(-17)	3.76(-17)	2.92(-17)	1.42(-17)
37.4	9.0(-17)	3.91(-17)	3.39(-17)	1.69(-17)
40.8	9.8(-17)	4.07(-17)	3.86(-17)	1.86(-17)
47.6	1.1(-16)	3.91(-17)	4.15(-17)	2.06(-17)
54.4	1.19(-16)	4.52(-17)	4.76(-17)	2.52(-17)
61.2	1.25(-16)	4.74(-17)	5.0(-17)	2.6(-17)
68	1.29(-16)	4.77(-17)	5.28(-17)	2.7(-17)
81.6	1.34(-16)	4.95(-17)	5.5(-17)	2.8(-17)
95.2	1.35(-16)	4.95(-17)	5.5(-17)	2.8(-17)
108.8	1.34(-16)	0.37 σ_T	0.41 σ_T	0.21 σ_T
122.4	1.33(-16)			
136.2	1.30(-16)			
170	1.24(-16)			
204	1.17(-16)			
272	1.04(-16)			
408	8.57(-17)			
544	7.32(-17)			
680	6.4(-17)			
1020	4.9(-17)			
1360	4.1(-17)			

For $10^3 < E < 10^5$ use $\sigma_T = \frac{1.8\times10^{-14}}{E} \log (E/13.6)$

Table II — Electron Impact Excitation Cross Section of 0(1D) and 0(1S)

Energy(eV)	O(1D) σ ($10^{-17} cm^2$)
2.0	0
3.0	0.97
4.0	1.85
5.0	2.4
6.0	2.58
7.0	2.52
8.0	2.40
9.0	2.25
10.0	1.97

11.0 and higher E use $\sigma = 2.62 \times 10^{-14}/E^3$

Energy(eV)	O(1S) σ ($10^{-18} cm^2$)
4	0.98
5	1.3
6	1.8
7	1.97
8	2.0
9	2.37
10	2.6

11 and higher E use $\sigma = 3.46 \times 10^{-15}/E^3$

Table III — States with Optically Allowed Transitions to the Ground State

State	Excitation Energy (eV)	Oscillator Strength
3s $^3S^o$	9.5	0.046
3d $^3D^o$	12.10	0.01
3s' $^3D^o$	12.50	0.056
3s' $^3P^o$	14.10	0.037
3d' $^3P^o$	15.3	0.0077

Table IV — Electron Impact Excitation of $3_p - 5_s$

Energy	$\sigma(10^{-17}cm^2)$
10	0.107
11.2	1.17
15	2.5
20	1.62
40	0.42
50	0.25
55	0.2
Higher	$\sigma = 3.1x10^{-13}/E^3$

Table V — Cross Section Parameters for Rydberg and Other Forbidden States

σ	E_{ij}	c	f_{ij}	ν	Ω
σ_{R1}	11.93	0.018	1.5	2.5	0.7
σ_{R2}	12.76	0.008	1.5	2.5	0.7
σ_{R3}	16.11	0.0065	1.5	2.5	0.7
σ_{R4}	11.0	0.053	0.07	0.5	0.7
σ_{R5}	14.5	0.065	0.07	0.5	0.7
σ_{R6}	15.8	0.043	0.07	0.5	0.7
σ_{R7}	14.1	0.055	0.1	1.0	1.0
σ_{R8}	10.7	0.068	0.3	1.0	2.0
σ_{R9}	14.0	0.08	0.3	1.0	2.0
σ_{R10}	15.8	0.054	0.3	1.0	2.0
σ_{R11}	12.7	0.065	0.4	1.0	2.0
σ_{R12}	12.1	0.043	0.4	1.0	2.0
σ_{R13}	14.1	0.065	0.14	1.0	2.0

Table VI — Summary of Results

Incident Energy	500 eV	1 KeV	5KeV	10 KeV	50 KeV	100 KeV	500 KeV	1 MeV
Loss Function $L(E)$ ($eV\text{-}cm^2$)	2.78(-15)	1.92(-15)	6.83(-16)	4.12(-16)	1.20(-16)	6.92(-17)	1.86(-17)	1.04(-17)
Energy per ion pair W_i (eV)	27.7	27.1	27.7	27.8	27.8	27.8	27.9	28.0
% of ion pairs due to 1st generation secondaries	75	69	57	53	46	43	38	36
% of ion pairs due to the rest of secondaries	25	31	43	47	54	57	62	64
% of beam deposition in excitation	8	5	6	5	5	4	4	4
% of beam deposition in ionization	44	41	33	31	26	25	22	21
% of beam deposition in 1st generation secondary energy	48	54	61	64	69	71	74	75

(Rows 4-6 are the 3 forbidden states. Rows 7-11 are the optically allowed states in the order given in Table III.)

500 eV

Species		Dir	Sec	Total
O+4S		0.281	0.119	0.400
O+2D		0.311	0.088	0.399
O+2P		0.160	0.042	0.202
O	1-2F	0.000	2.017	2.017
O	1-3F	0.000	0.062	0.062
O	1-4F	0.000	0.125	0.125
O	1-4	0.103	0.198	0.300
O	1-5	0.008	0.008	0.016
O	1-6	0.042	0.041	0.084
O	1-7	0.024	0.018	0.042
O	1-8	0.005	0.003	0.008
O	R 1	0.008	0.006	0.014
O	R 2	0.003	0.002	0.005
O	R 3	0.002	0.001	0.003
O	R 4	0.001	0.005	0.006
O	R 5	0.001	0.002	0.003
O	R 6	0.001	0.001	0.002
O	R 7	0.000	0.001	0.002
O	R 8	0.000	0.009	0.009
O	R 9	0.000	0.003	0.003
O	R10	0.000	0.001	0.001
O	R11	0.000	0.005	0.006
O	R12	0.000	0.004	0.004
O	R13	0.000	0.001	0.001

1 KeV

Species		Dir	Sec	Total
O+4S		0.258	0.142	0.400
O+2D		0.286	0.113	0.399
O+2P		0.147	0.054	0.201
O	1-2F	0.000	2.018	2.018
O	1-3F	0.000	0.063	0.063
O	1-4F	0.000	0.126	0.126
O	1-4	0.060	0.211	0.272
O	1-5	0.005	0.009	0.014
O	1-6	0.025	0.046	0.072
O	1-7	0.014	0.021	0.035
O	1-8	0.003	0.003	0.006
O	R 1	0.006	0.007	0.012
O	R 2	0.002	0.002	0.005
O	R 3	0.001	0.001	0.002
O	R 4	0.001	0.005	0.006
O	R 5	0.001	0.002	0.003
O	R 6	0.000	0.001	0.002
O	R 7	0.000	0.001	0.002
O	R 8	0.000	0.009	0.009
O	R 9	0.000	0.004	0.004
O	R10	0.000	0.002	0.002
O	R11	0.000	0.006	0.006
O	R12	0.000	0.004	0.004
O	R13	0.000	0.001	0.001

5 KeV

Species		Dir	Sec	Total
O+4S		0.215	0.186	0.401
O+2D		0.238	0.161	0.399
O+2P		0.122	0.079	0.201
O	1-2F	0.000	2.020	2.020
O	1-3F	0.000	0.063	0.063
O	1-4F	0.000	0.127	0.127
O	1-4	0.069	0.231	0.300
O	1-5	0.005	0.011	0.016
O	1-6	0.029	0.054	0.083
O	1-7	0.017	0.025	0.042
O	1-8	0.003	0.004	0.008
O	R 1	0.007	0.008	0.015
O	R 2	0.003	0.003	0.006
O	R 3	0.002	0.001	0.003
O	R 4	0.001	0.006	0.007
O	R 5	0.001	0.003	0.003
O	R 6	0.001	0.001	0.002
O	R 7	0.000	0.002	0.002
O	R 8	0.000	0.009	0.009
O	R 9	0.000	0.004	0.004
O	R10	0.000	0.002	0.002
O	R11	0.000	0.006	0.006
O	R12	0.000	0.004	0.004
O	R13	0.000	0.001	0.001

10 KeV

Species		Dir	Sec	Total
O+4S		0.200	0.201	0.401
O+2D		0.221	0.178	0.399
O+2P		0.113	0.087	0.201
O	1-2F	0.000	2.020	2.020
O	1-3F	0.000	0.063	0.063
O	1-4F	0.000	0.127	0.127
O	1-4	0.063	0.237	0.300
O	1-5	0.005	0.011	0.016
O	1-6	0.027	0.056	0.083
O	1-7	0.016	0.026	0.042
O	1-8	0.003	0.005	0.008
O	R 1	0.007	0.009	0.016
O	R 2	0.003	0.003	0.006
O	R 3	0.002	0.001	0.003
O	R 4	0.001	0.006	0.007
O	R 5	0.001	0.003	0.004
O	R 6	0.001	0.001	0.002
O	R 7	0.000	0.002	0.002
O	R 8	0.000	0.009	0.009
O	R 9	0.000	0.004	0.004
O	R10	0.000	0.002	0.002
O	R11	0.000	0.006	0.006
O	R12	0.000	0.004	0.004
O	R13	0.000	0.001	0.001

50 KeV

Species	Dir	Sec	Total
O+4S	0.171	0.230	0.400
O+2D	0.189	0.209	0.399
O+2P	0.097	0.104	0.201
O 1-2F	0.000	2.024	2.024
O 1-3F	0.000	0.063	0.063
O 1-4F	0.000	0.126	0.126
O 1-4	0.053	0.247	0.300
O 1-5	0.004	0.012	0.016
O 1-6	0.023	0.061	0.083
O 1-7	0.013	0.029	0.042
O 1-8	0.003	0.005	0.008
O R 1	0.008	0.010	0.018
O R 2	0.003	0.004	0.007
O R 3	0.002	0.002	0.004
O R 4	0.001	0.006	0.007
O R 5	0.001	0.003	0.004
O R 6	0.001	0.001	0.002
O R 7	0.000	0.002	0.002
O R 8	0.000	0.009	0.009
O R 9	0.000	0.004	0.004
O R10	0.000	0.002	0.002
O R11	0.000	0.006	0.006
O R12	0.000	0.004	0.004
O R13	0.000	0.001	0.001

100 KeV

Species	Dir	Sec	Total
O+4S	0.161	0.240	0.401
O+2D	0.178	0.220	0.399
O+2P	0.091	0.109	0.201
O 1-2F	0.000	2.019	2.019
O 1-3F	0.000	0.063	0.063
O 1-4F	0.000	0.127	0.127
O 1-4	0.050	0.251	0.301
O 1-5	0.004	0.012	0.016
O 1-6	0.021	0.062	0.084
O 1-7	0.012	0.029	0.042
O 1-8	0.002	0.005	0.008
O R 1	0.009	0.010	0.019
O R 2	0.004	0.004	0.007
O R 3	0.002	0.002	0.004
O R 4	0.001	0.006	0.007
O R 5	0.001	0.003	0.004
O R 6	0.001	0.001	0.002
O R 7	0.000	0.002	0.002
O R 8	0.000	0.009	0.009
O R 9	0.000	0.004	0.004
O R10	0.000	0.002	0.002
O R11	0.000	0.006	0.006
O R12	0.000	0.004	0.004
O R13	0.000	0.001	0.001

500 KeV

Species		Dir	Sec	Total
O+4S		0.142	0.259	0.401
O+2D		0.157	0.242	0.398
O+2P		0.081	0.120	0.201
O	1-2F	0.000	2.022	2.022
O	1-3F	0.000	0.063	0.063
O	1-4F	0.000	0.127	0.127
O	1-4	0.044	0.257	0.301
O	1-5	0.003	0.013	0.016
O	1-6	0.019	0.065	0.084
O	1-7	0.011	0.031	0.042
O	1-8	0.002	0.005	0.008
O	R 1	0.011	0.011	0.022
O	R 2	0.004	0.004	0.009
O	R 3	0.003	0.002	0.005
O	R 4	0.002	0.006	0.008
O	R 5	0.001	0.003	0.004
O	R 6	0.001	0.001	0.002
O	R 7	0.000	0.002	0.002
O	R 8	0.000	0.009	0.009
O	R 9	0.000	0.004	0.004
O	R10	0.000	0.002	0.002
O	R11	0.000	0.006	0.006
O	R12	0.000	0.004	0.004
O	R13	0.000	0.001	0.001

1 MeV

Species		Dir	Sec	Total
O+4S		0.135	0.266	0.401
O+2D		0.149	0.249	0.398
O+2P		0.077	0.124	0.201
O	1-2F	0.000	2.019	2.019
O	1-3F	0.000	0.063	0.063
O	1-4F	0.000	0.127	0.127
O	1-4	0.041	0.260	0.301
O	1-5	0.003	0.013	0.016
O	1-6	0.018	0.066	0.084
O	1-7	0.010	0.032	0.042
O	1-8	0.002	0.006	0.008
O	R 1	0.012	0.011	0.023
O	R 2	0.005	0.004	0.009
O	R 3	0.003	0.002	0.005
O	R 4	0.002	0.006	0.008
O	R 5	0.002	0.003	0.005
O	R 6	0.001	0.002	0.002
O	R 7	0.000	0.002	0.002
O	R 8	0.000	0.009	0.009
O	R 9	0.000	0.004	0.004
O	R10	0.000	0.002	0.002
O	R11	0.000	0.006	0.006
O	R12	0.000	0.004	0.004
O	R13	0.000	0.001	0.001

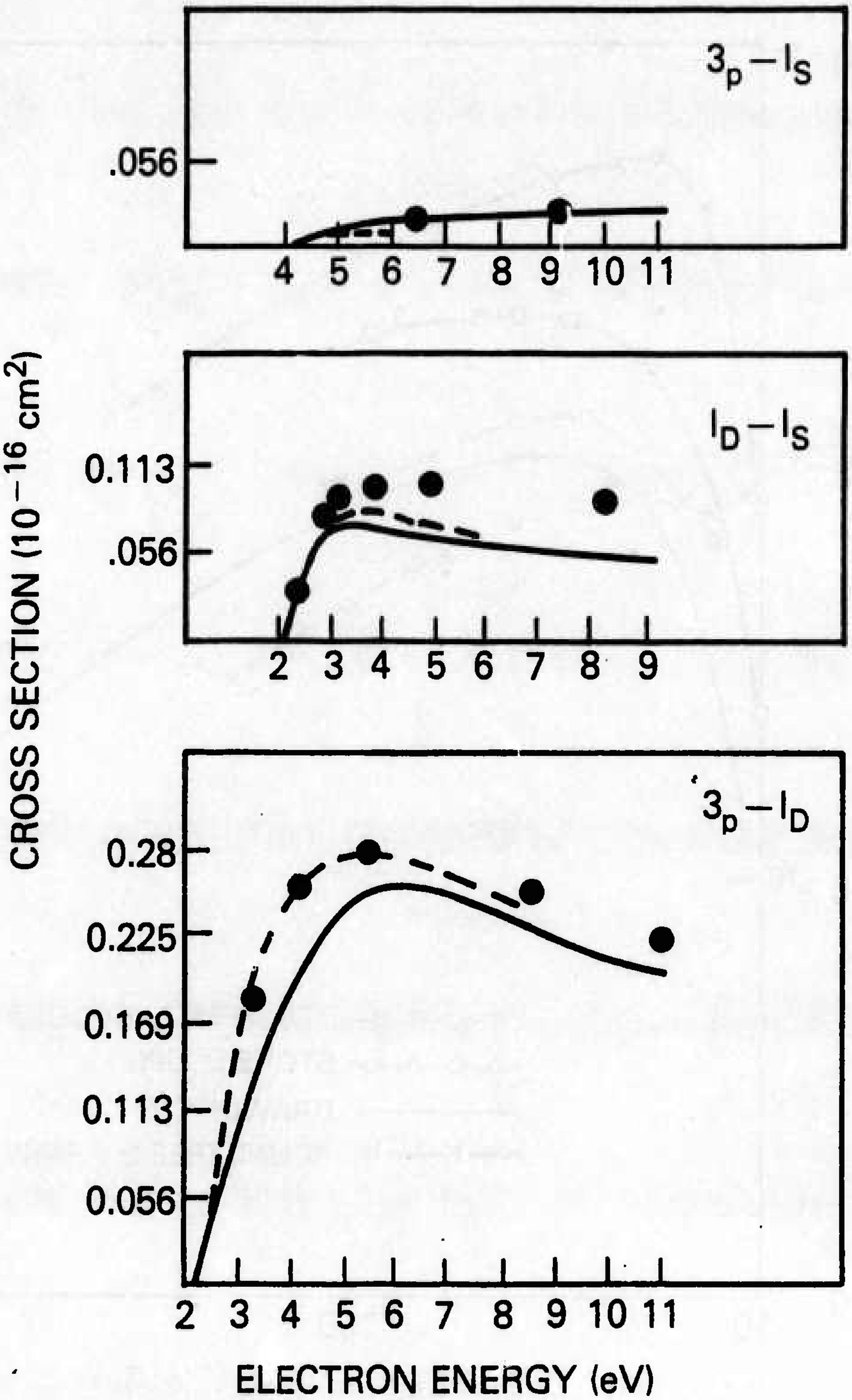

Fig. 1 — Electron impact excitation cross section for low lying metastable states of oxygen, solid curve (Ref. 23) and dashed lines (Ref. 35).

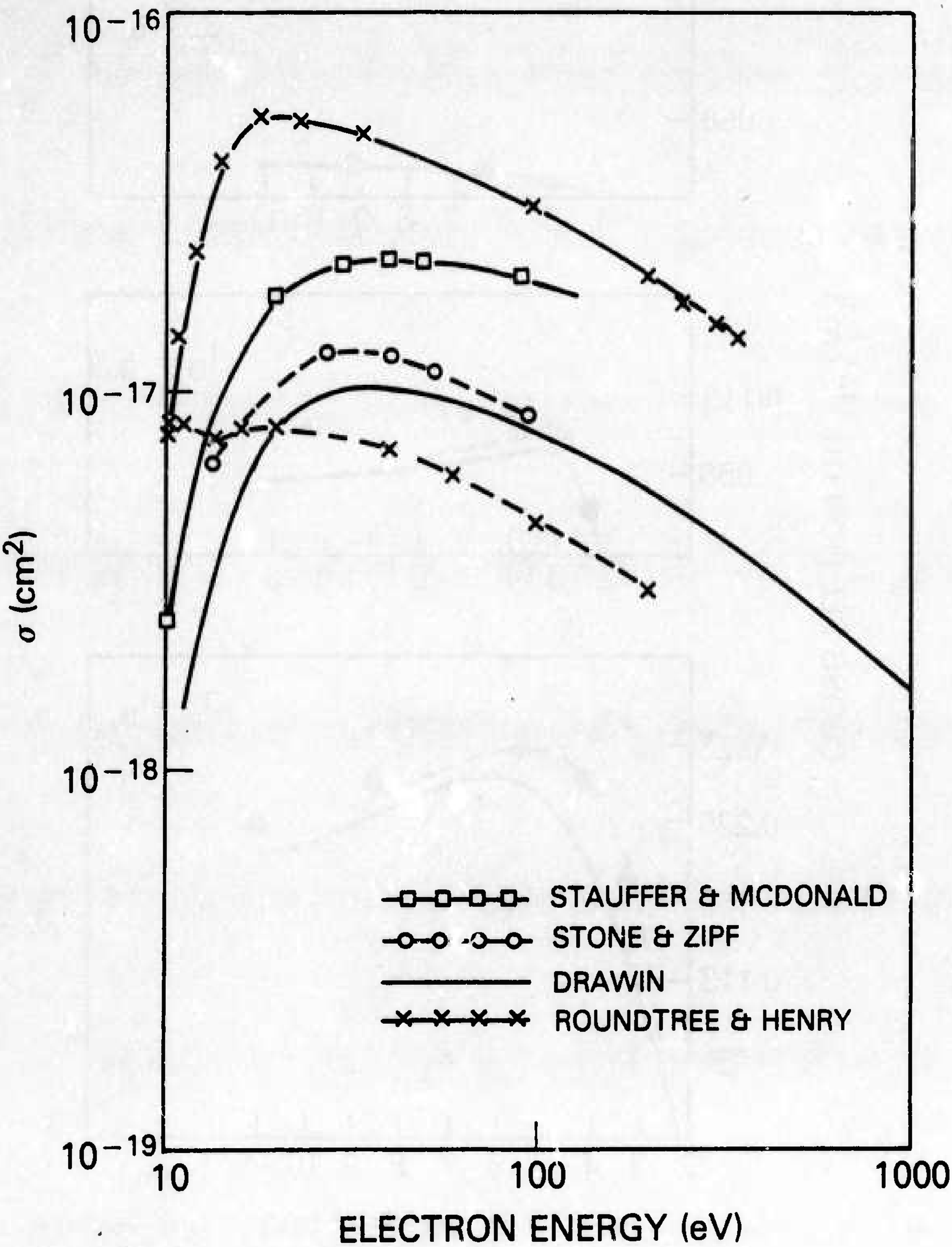

Fig. 2 — Electron impact excitation of the oxygen resonance line. ($3_P - 3_S$)

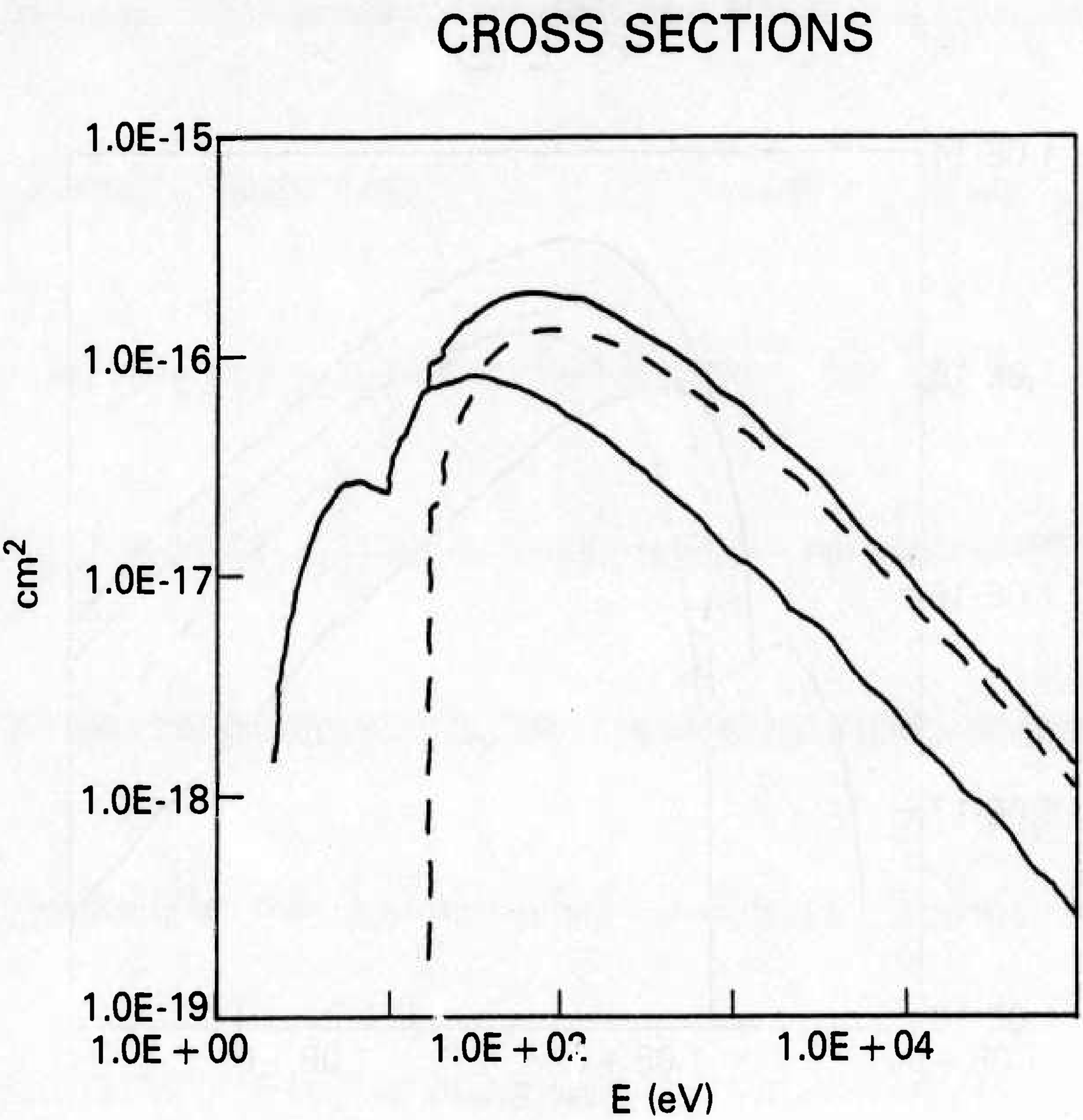

Fig. 3 — Total cross sections in atomic oxygen. The lower solid line is for electronic excitation. The dashed is for ionization.

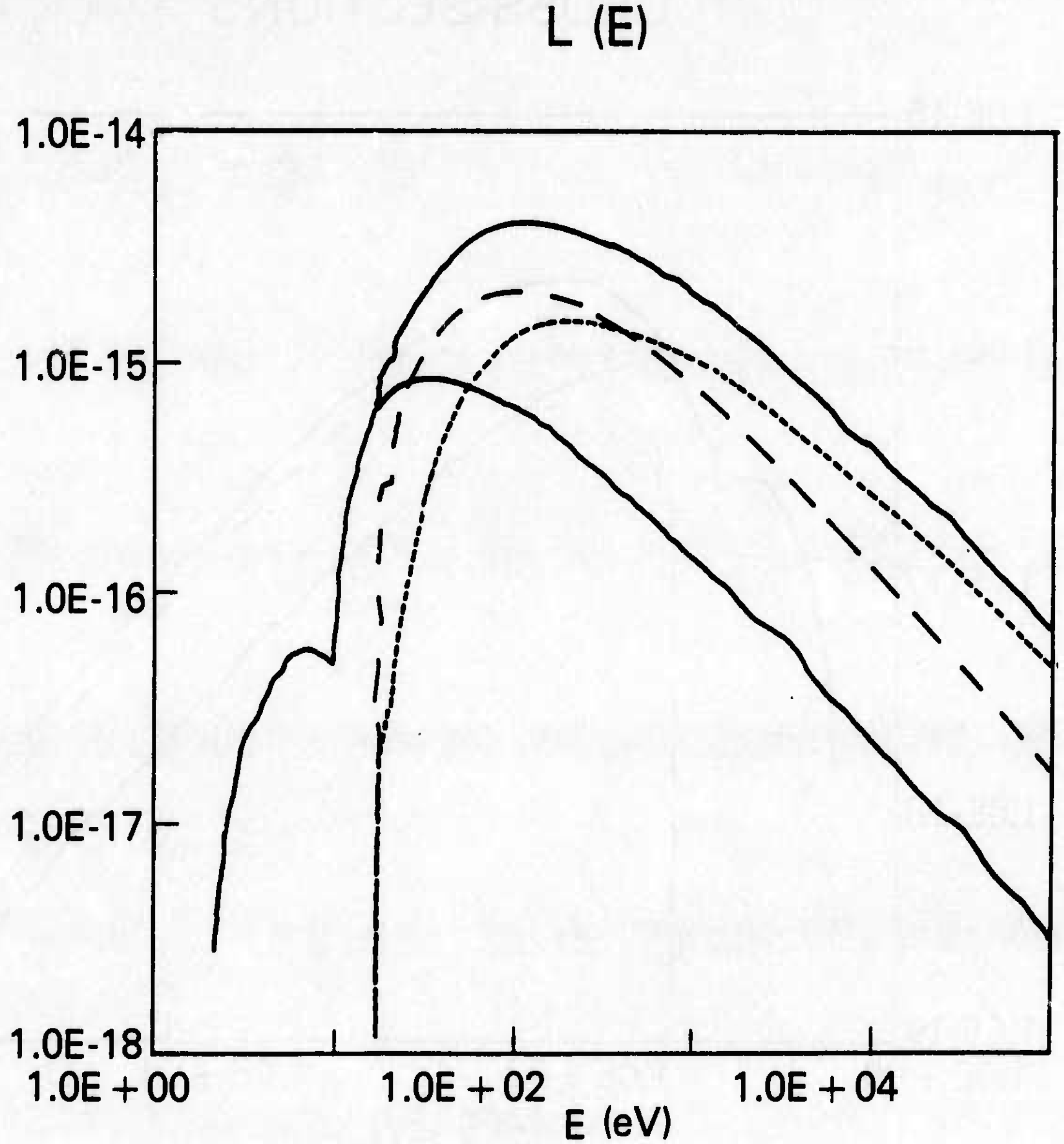

Fig. 4 — The loss function in atomic oxygen. The solid line is loss to electronic excitations. The dashed line is loss to ionization. The dotted line is to secondary electrons.

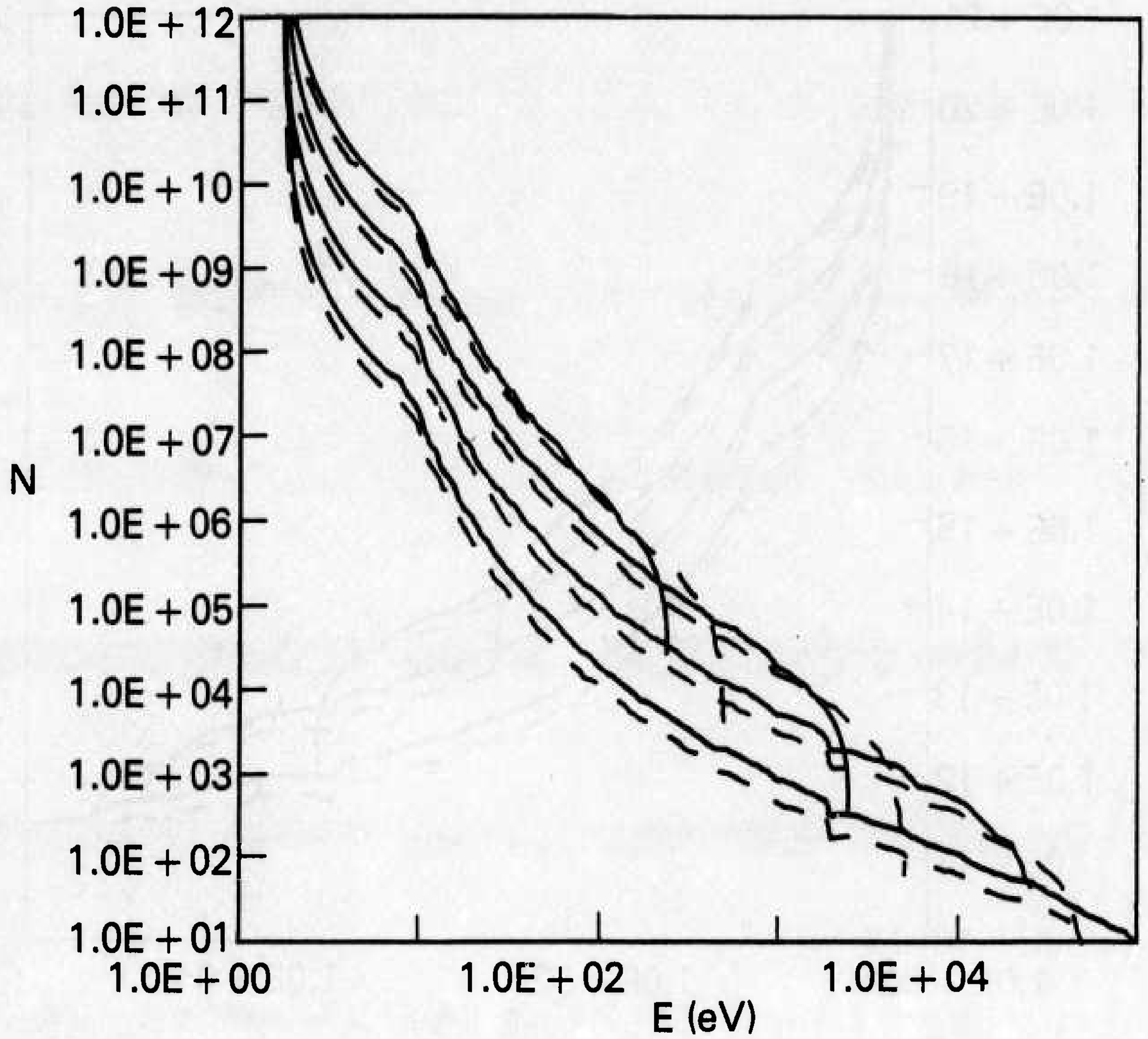

Fig. 5 — Steady state secondary electron distribution function for beam electrons with energies of 500 to 1 MeV.

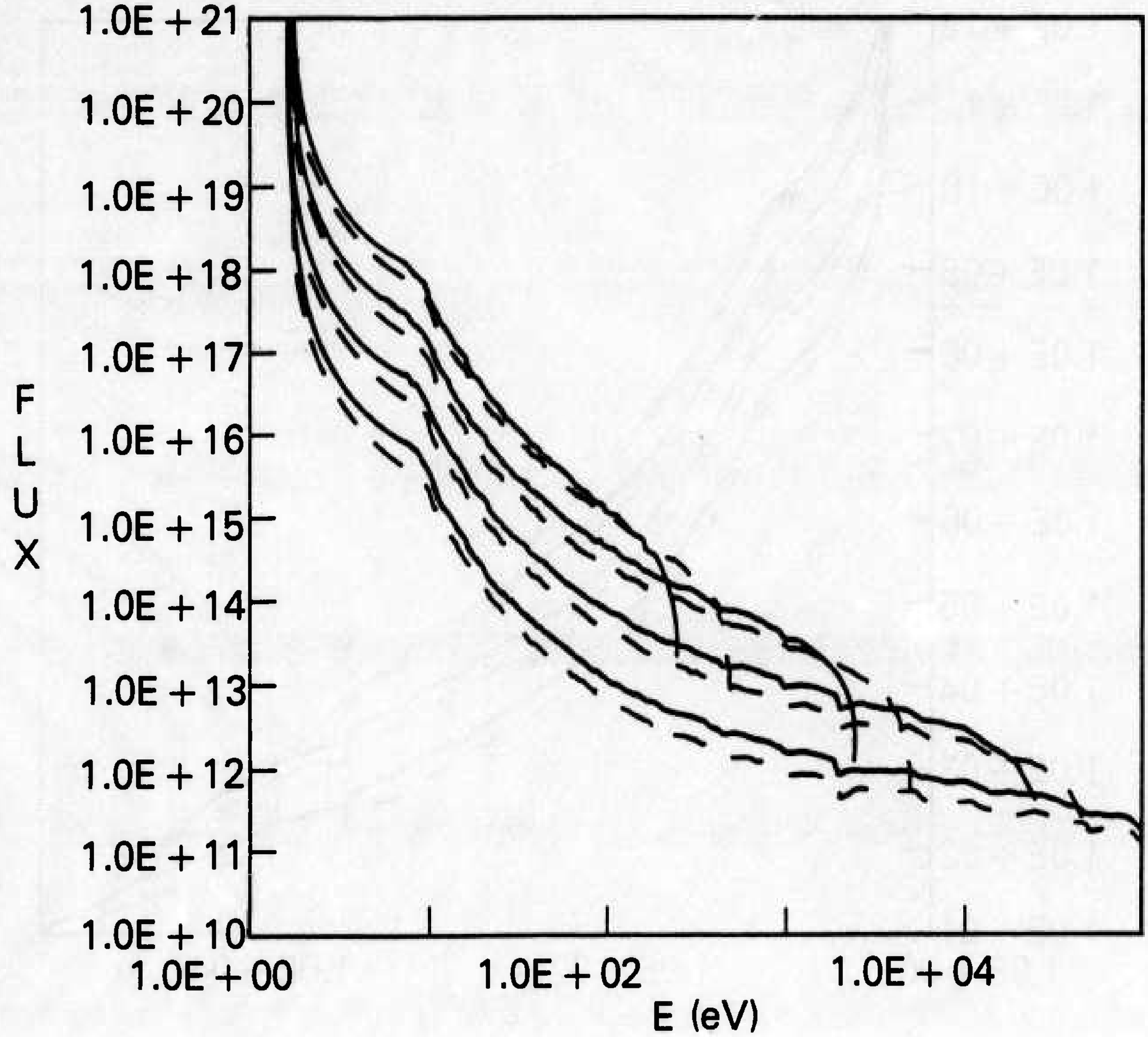

Fig. 6 — Steady state secondary electron flux for beam electron energies of 500 to 1 MeV.

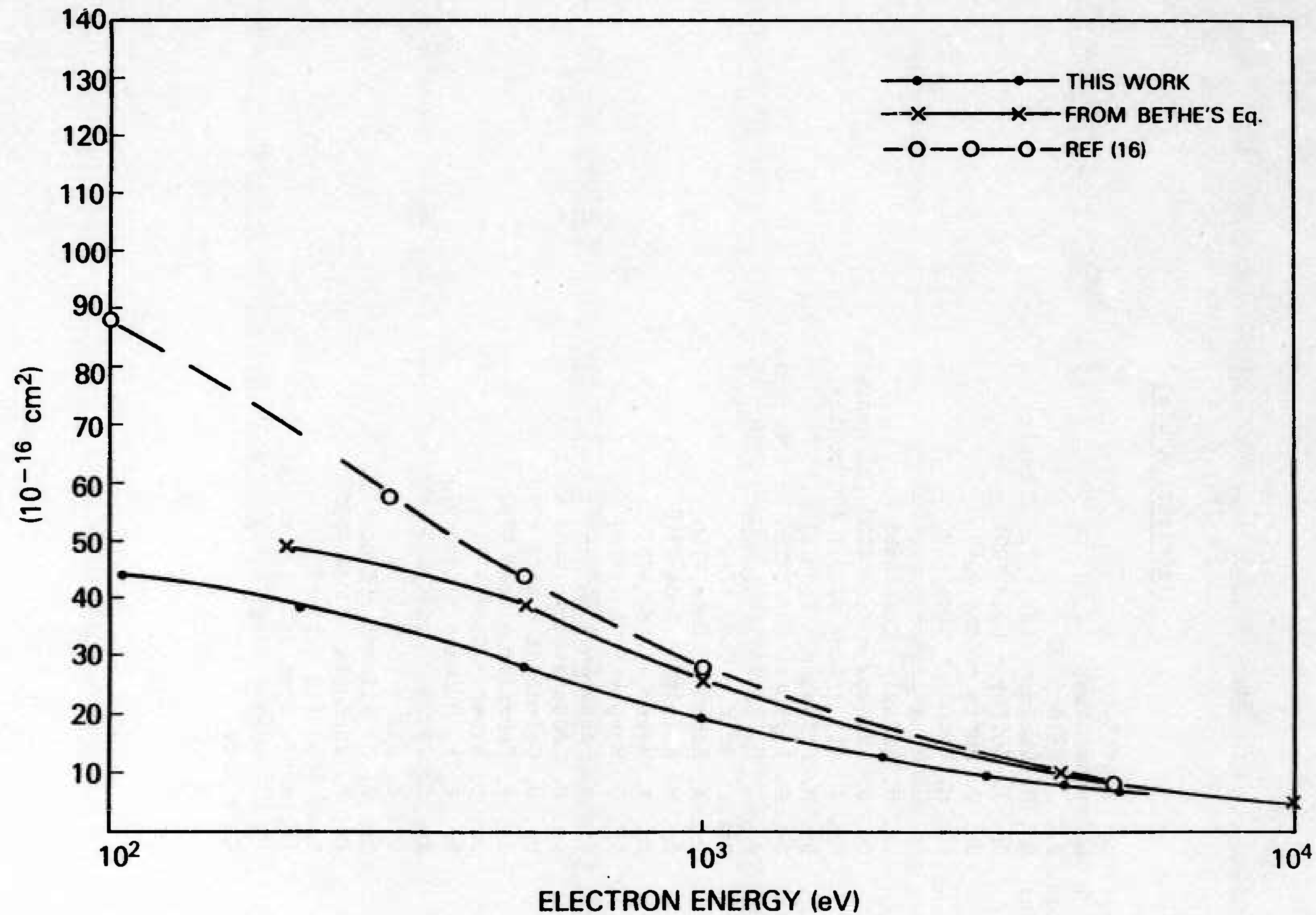

Fig. 7 — Loss function in atomic oxygen. (a comparison)

Distribution List

Naval Research Laboratory
4555 Overlook Avenue, S.W.
Washington, D.C. 20375-5000

Attn: Dr. M. Lampe - Code 4792 (2 copies)
Dr. T. Coffey - Code 1001
Dr. J. Boris - Code 4040
Dr. M. Picone - Code 4040
Dr. J. B. Aviles - Code 4665
Dr. M. Haftel - Code 4665
Dr. S. Ossakow - Code 4700 (26 copies)
Dr. A. Ali - Code 4700.1 (30 copies)
Dr. M. Friedman - Code 4700.1
Dr. R. Taylor - BRA (4700.1) (30 copies)
Mr. I. M. Vitkovitsky - Code 4701
Dr. S. Gold - Code 4740
Dr. A. Robson - Code 4760
Dr. M. Raleigh - Code 4760
Dr. R. Meger - Code 4763
Dr. D. Murphy - Code 4763
Dr. R. Pechacek - Code 4763
Dr. G. Cooperstein - Code 4770
Dr. D. Colombant - Code 4790
Dr. R. Fernsler - Code 4790
Dr. I. Haber - Code 4790
Dr. R. F. Hubbard - Code 4790
Dr. G. Joyce - Code 4790
Dr. Y. Lau - Code 4790
Dr. S. P. Slinker - Code 4790
Dr. P. Sprangle - Code 4790
Code 4790 (20 copies)
Library - Code 2628 (20 copies)
D. Wilbanks - Code 2634
Code 1220

Air Force Office of Scientific Research
Physical and Geophysical Sciences
Bolling Air Force Base
Washington, DC 20332
Attn: Major Bruce Smith

Air Force Weapons Laboratory
Kirtland Air Force Base
Albuquerque, NM 87117
Attn: C. Clark (AFWL/NTYP)
W. Baker (AFWL/NTYP)
D. Dietz (AFWL/NTYP)
Lt Col J. Head

U. S. Army Ballistics Research Laboratory
Aberdeen Proving Ground, Maryland 21005
Attn: Dr. Donald Eccleshall (DRXBR-BM)
Dr. Anand Prakash

Avco Everett Research Laboratory
2385 Revere Beach Pkwy
Everett, Massachusetts 02149
Attn: Dr. R. Patrick
Dr. Dennis Reilly

Ballistic Missile Def. Ad. Tech. Ctr.
P.O. Box 1500
Huntsville, Alabama 35807
Attn: Dr. M. Hawie (BMDSATC-1)

Chief of Naval Material
Office of Naval Technology
MAT-0712, Room 503
800 North Quincy Street
Arlington, VA 22217
Attn: Dr. Eli Zimet

Cornell University
Ithaca, NY 14853
Attn: Prof. David Hammer

DASIAC - DETIR
Kaman Tempo
25600 Huntington Avenue, Suite 500
Alexandria, VA 22303
Attn: Mr. F. Wimenitz

Defense Advanced Research Projects Agency
1400 Wilson Blvd.
Arlington, VA 22209
Attn: Dr. Shen Shey
Dr. H. L. Buchanan

Defense Technical Information Center
Cameron Station
5010 Duke Street
Alexandria, VA 22314 (2 copies)

Department of Energy
Washington, DC 20545
Attn: Dr. Terry F. Godlove (ER20:GTN,
High Energy and Nuclear Physics)
Mr. Gerald J. Peters (G-256)

Directed Technologies, Inc.
226 Potomac School Road
McLean, VA 22101
Attn: Dr. Ira F. Kuhn
Dr. Nancy Chesser

C. S. Draper Laboratories
555 Technology Square
Cambridge, Massachusetts 02139
Attn: Dr. E. Olsson
Dr. L. Matson

Institute for Fusion Studies
University of Texas at Austin
RLM 11.218
Austin, TX 78712
Attn: Prof. Marshall N. Rosenbluth

Intelcom Rad Tech.
P.O. Box 81087
San Diego, California 92138
Attn: Dr. W. Selph

Joint Institute for Laboratory
Astrophysics
National Bureau of Standards and
University of Colorado
Boulder, CO 80309
Attn: Dr. Arthur V. Phelps

Kaman Sciences
1500 Garden of the Gods Road
Colorado Springs, CO 80933
Attn: Dr. John P. Jackson

Lawrence Berkeley Laboratory
University of California
Berkeley, CA 94720
Attn: Dr. Edward P. Lee

Lawrence Livermore National Laboratory
University of California
Livermore, California 94550
Attn Dr. Richard J. Briggs
Dr. Simon S. Yu
Dr. Frank Chambers
Dr. James W.-K. Mark, L-477
Dr. William Fawley
Dr. William Barletta
Dr. William Sharp
Dr. Daniel S. Prono
Dr. John K. Boyd
Dr. Kenneth W. Struve
Dr. John Clark
Dr. George J. Caporaso
Dr. William E. Martin
Dr. Donald Prosnitz

Lockheed Palo Alto Laboratory
3251 Hanover St.
Bldg. 203, Dept 52-11
Palo Alto, CA 94304
Attn: Dr. John Siambis

Los Alamos National Scientific Laboratory
P.O. Box 1663
Los Alamos, NM 87545
Attn: Dr. L. Thode
Dr. M. A. Mostrom, MS-608
Dr. H. Dogliani, MS-5000
Dr. R. Carlson
Ms. Leah Baker, MS-P940
Dr. Carl Ekdahl

Maxwell Laboratories Inc.
8888 Balboa Avenue
San Diego, CA 92123
Attn: Dr. Ken Whitham

McDonnell Douglas Research Laboratories
Dept. 223, Bldg. 33, Level 45
Box 516
St. Louis, MO 63166
Attn: Dr. Evan Rose
Dr. Carl Leader

Mission Research Corporation
EM Systems Applications
1720 Randolph Road, S.E.
Albuquerque, NM 87106
Attn: Dr. Brendan Godfrey
Dr. Thomas Hughes
Dr. Lawrence Wright
Dr. A. B. Newberger

Mission Research Corporation
P. O. Drawer 719
Santa Barbara, California 93102
Attn: Dr. C. Longmire
Dr. N. Carron

National Bureau of Standards
Gaithersburg, Maryland 20760
Attn: Dr. Mark Wilson

Naval Surface Weapons Center
White Oak Laboratory
Silver Spring, Maryland 20903-5000
Attn: Dr. R. Cawley
Dr. J. W. Forbes
Dr. E. E. Nolting
Mr. W. M. Hinckley
Mr. N. E. Scofield
Dr. E. C. Whitman
Dr. M. H. Cha
Dr. H. S. Uhm
Dr. R. Fiorito
Dr. K. T. Nguyen
Dr. R. Stark
Dr. R. Chen

Office of Naval Research
800 North Quincy Street
Arlington, VA 22217
Attn: Dr. C. W. Roberson
Dr. W. S. Condell (Code 421)

Office of Under Secretary of Defense
Research and Engineering
Room 3E1034
The Pentagon
Washington, DC 20301
Attn: Mr. John M. Bachkosky

ORI, Inc.
1375 Piccard Drive
Rockville, MD 20850
Attn: Dr. C. M. Huddleston

Physical Dynamics, Inc.
P.O. Box 1883
La Jolla, California 92038
Attn: Dr. K. Brueckner

Physics International, Inc.
2700 Merced Street
San Leandro, CA. 94577
Attn: Dr. E. Goldman

Princeton University
Plasma Physics Laboratory
Princeton, NJ 08540
Attn: Dr. Francis Perkins, Jr.

Pulse Sciences, Inc.
14796 Wicks Blvd.
San Leandro, CA 94577
Attn: Dr. Sidney Putnam
Dr. John Bayless

Sandia National Laboratory
Albuquerque, NM 87115
Attn: Dr. Bruce Miller
Dr. Barbara Epstein
Dr. John Freeman
Dr. Gordon T. Leifeste
Dr. Gerald N. Hays
Dr. James Chang
Dr. Michael G. Mazerakis
Dr. John Wagner
Dr. Ron Lipinski

Science Applications Intl. Corp.
5150 El Camino Road
Los Altos, CA 94022
Attn: Dr. R. R. Johnston
Dr. Leon Feinstein
Dr. Douglas Keeley

Science Applications Intl. Corp.
1710 Goodridge Drive
McLean, VA 22102
Attn: Mr. W. Chadsey
Dr. A Drobot
Dr. K. Papadopoulos
Dr. B. Hui

Commander
Space & Naval Warfare Systems Command
PMW-145
Washington, DC 20363-5100
Attn: CAPT J. D. Fontana
CDR W. Bassett

SRI International
PSO-15
Molecular Physics Laboratory
333 Ravenswood Avenue
Menlo Park, CA 94025
Attn: Dr. Donald Eckstrom

Strategic Defense Initiative Org.
1717 H Street, N. W.
Washington, DC 20009
Attn: Lt Col R. L. Gullickson
Dr. J. Ionson
Dr. D. Duston

Strategic Defense Initiative Office
Directed Energy Weapons Office, The Pentagon
Office of the Secretary of Defense
Washington, DC 20301-7100
Attn: Dr. C. F. Sharn (OP0987B)

Titan Systems, Inc.
8950 Villa La Jolla Drive-Suite 2232
La Jolla, CA 92037
Attn: Dr. R. M. Dowe

University of California
Physics Department
Irvine, CA 92664
Attn: Dr. Gregory Benford
University of Maryland
Physics Department
College Park, MD 20742
Attn: Dr. Y. C. Lee
Dr. C. Grebogi

University of Michigan
Dept. of Nuclear Engineering
Ann Arbor, MI 48109
Attn: Prof. Terry Kammash
Prof. R. Gilgenbach

Director of Research
U.S. Naval Academy
Annapolis, MD 21402 (2copies)